Supplementary Information

Accurate Inverse Process Optimization Framework in Laser Directed Energy Deposition

Xiao Shang[1], Ajay Talbot[1], Evelyn Li[1], Haitao Wen[1], Tianyi Lyu[1], Jiahui Zhang[1], Yu Zou[1] *

[1]Department of Materials Science and Engineering, University of Toronto, Toronto, ON, Canada, M5S 3E4
*Corresponding author. Email: mse.zou@utoronto.ca

This file includes:

Figures S1 to S8

Tables S1 to S4

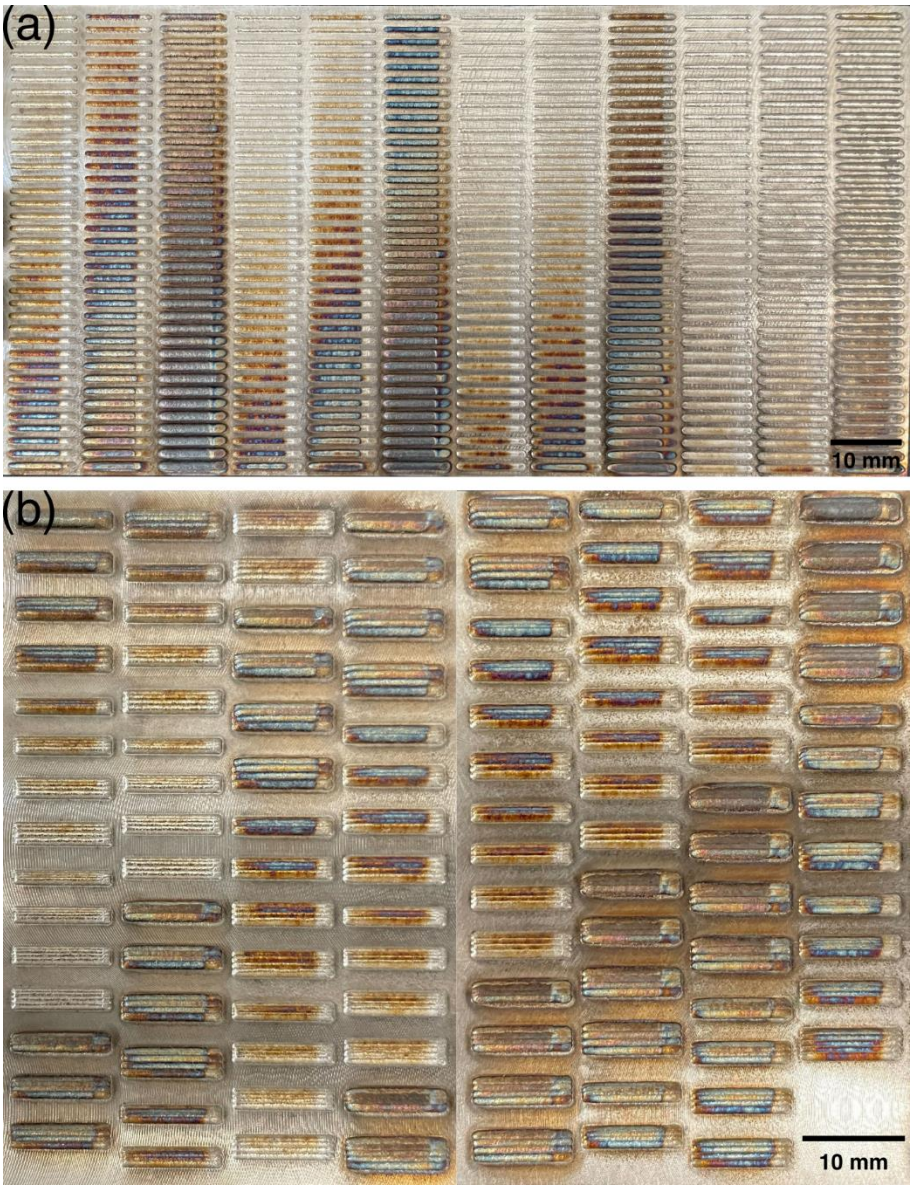

Figure S1. Top views of the single-track and multi-track prints in the dataset. (a) Single-track prints. (b) Multi-track prints.

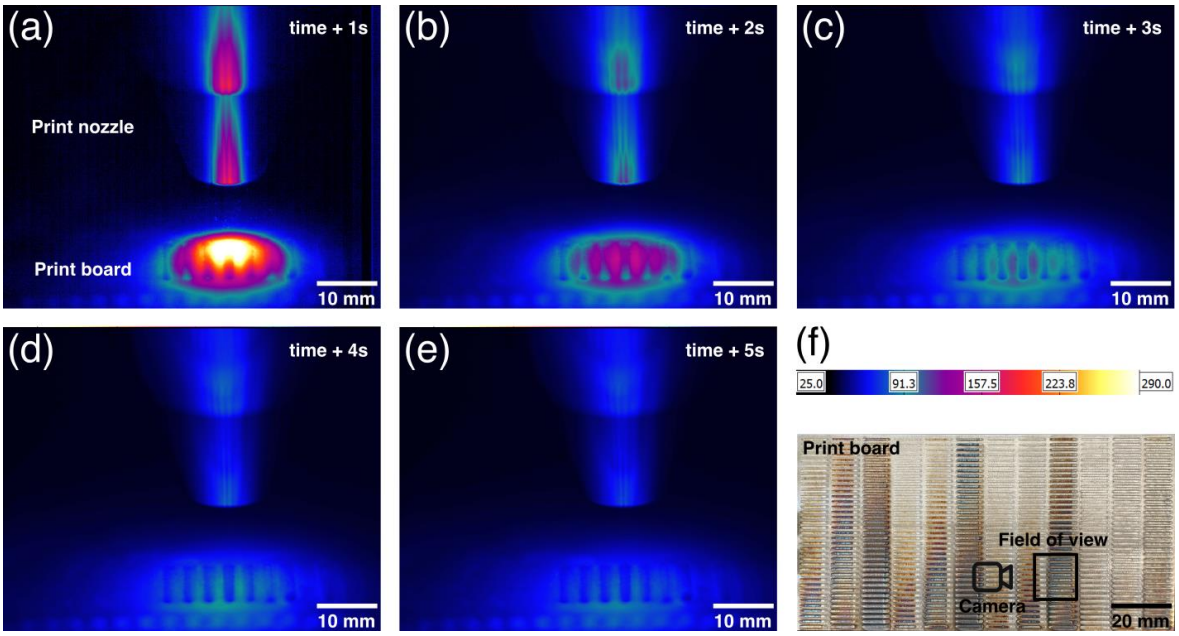

Figure S2. Infrared thermal (IR) images showing the temperature of the print board. (a)-(e) Temperature distributions on the print board at 1 s, 2 s, 3s, 4s, and 5s after the track being deposited, respectively. (f) Temperature colour bar and IR camera viewing sketch.

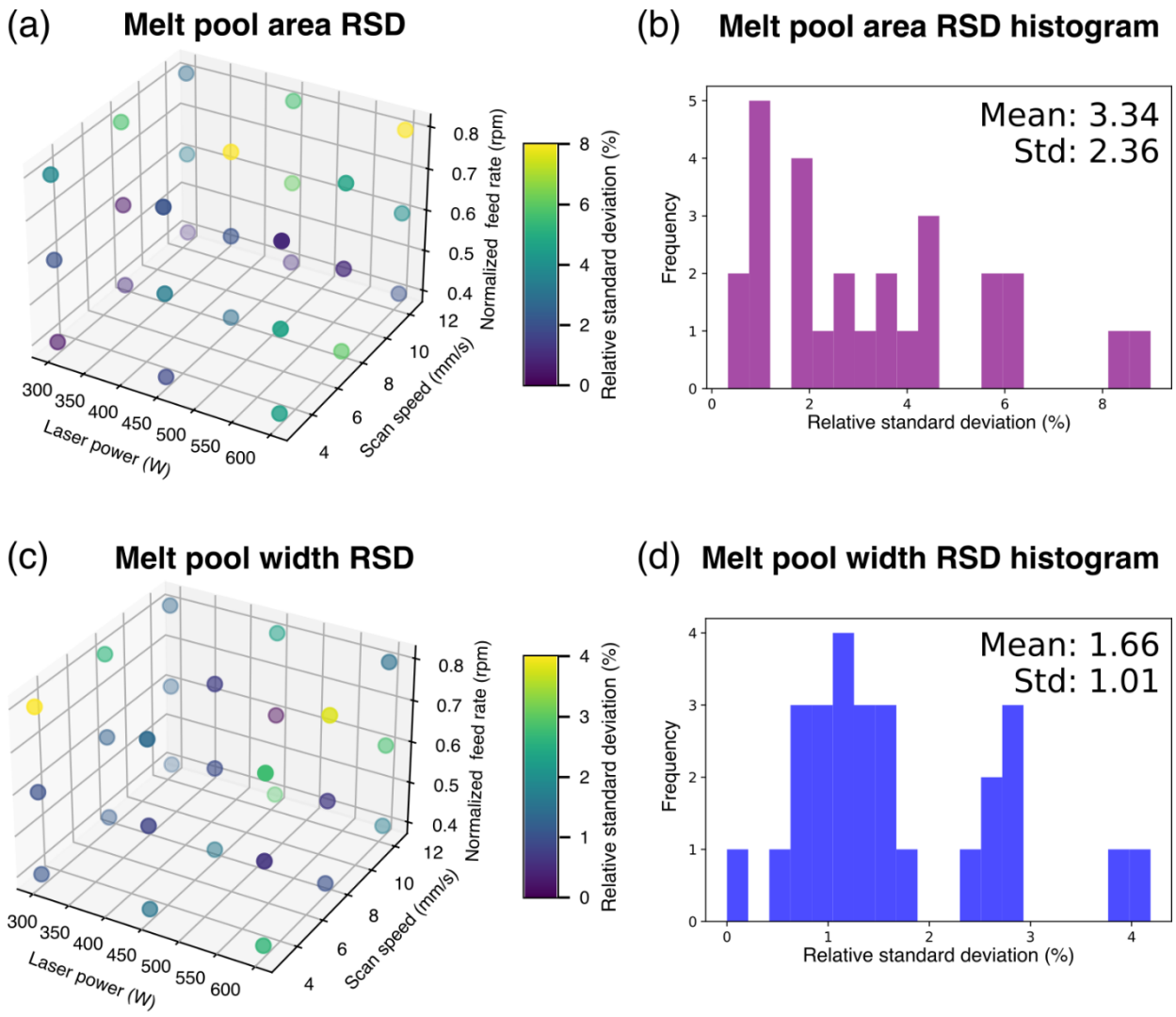

Figure S3. Single-track melt pool inconsistency study results. (a) and (c) The process parameter design space and the corresponding relative standard deviation (RSD) for the melt pool area and the melt pool width, respectively. (b) and (d) Histograms showing the distributions of the RSD values for the melt pool area and the melt pool width, respectively. The mean and standard deviation of both distributions are marked.

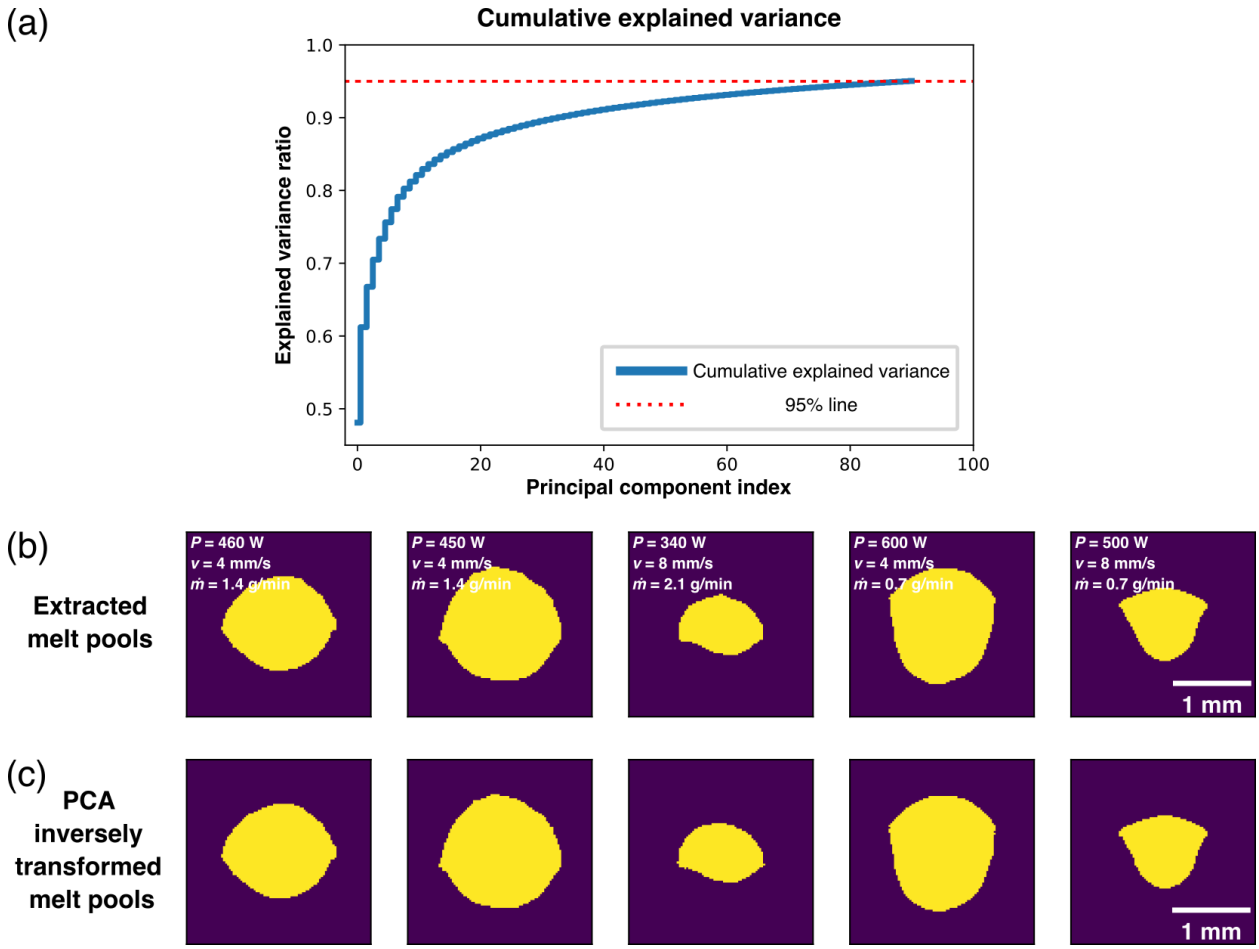

Figure S4. Cumulative explained variance during principal component analysis (PCA) and comparisons between melt pool contours before and after PCA. (a) Plot showing the cumulative explained variance during PCA. The red dotted line marks where 95% of the variance is preserved. (b) Melt pool contours directly extracted from optical microscopic images. (c) Melt pool contours inversely transformed after PCA.

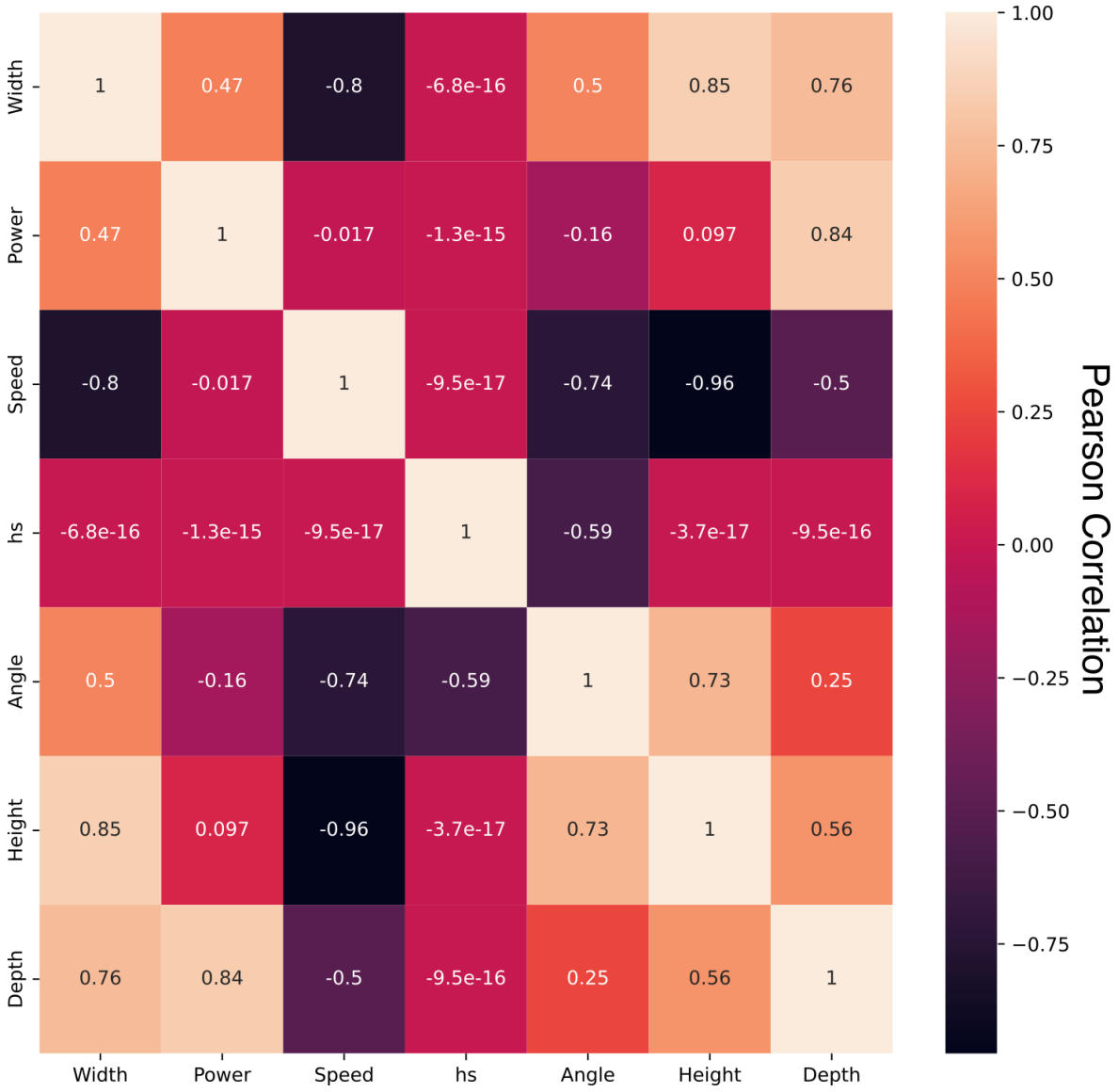

Figure S5. Correlation heat map between process parameters, single-track melt pool geometrical signatures, and the tilt angle. The Pearson correlation coefficient is calculated and shown on the heat map, with the exact coefficient value marked in each tile.

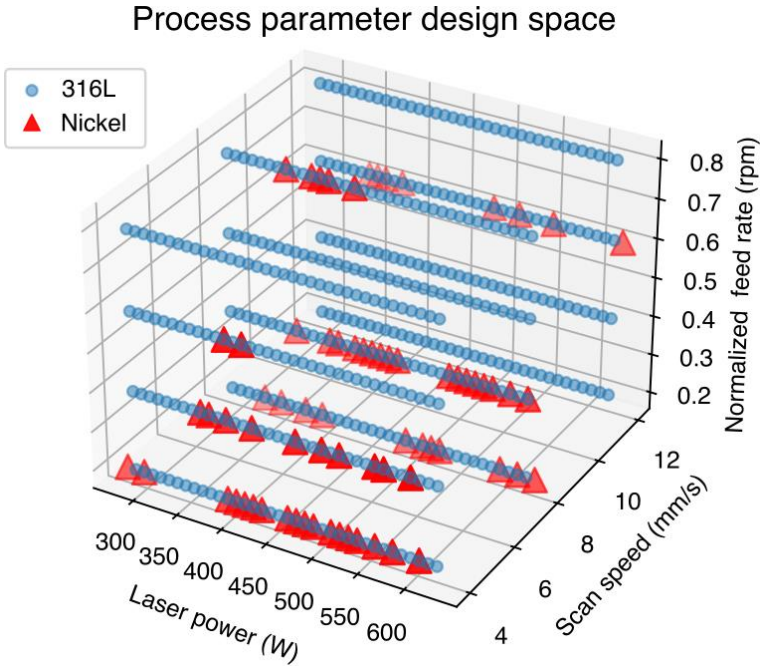

Figure S6. Process parameter design space of the pure nickel dataset in the 316L stainless steel dataset.

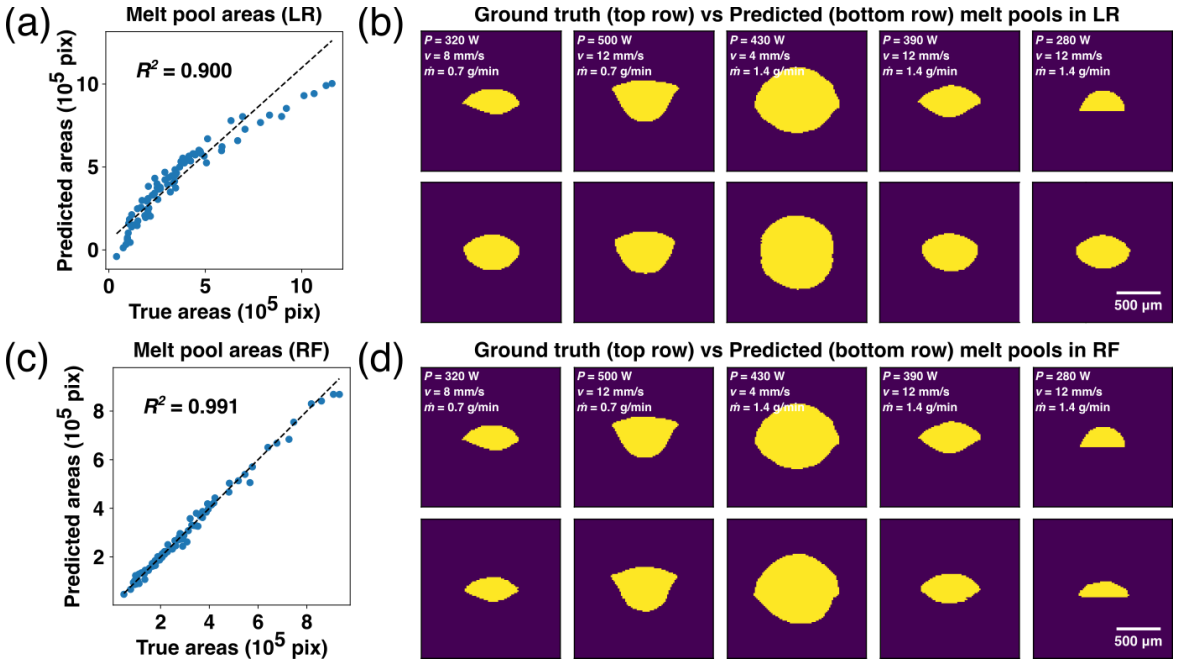

Figure S7. Model performance of two comparison models, i.e., linear regression (LR) and random forest (RF). (a) and (c) Parity plots of the two models in predicting the melt pool area. (b) and (d) Contour comparison of the two models between ground truth, i.e., extracted directly form microscopic images, and predicted.

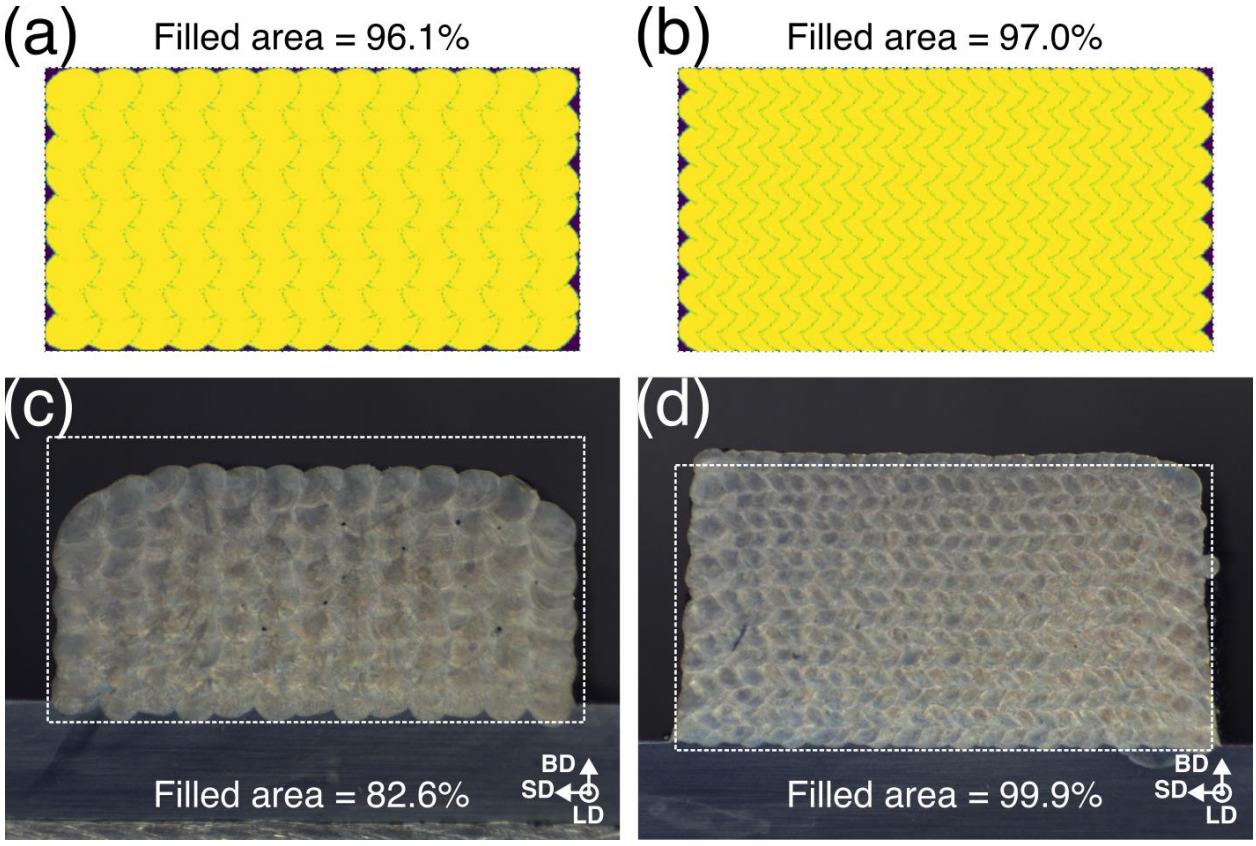

Figure S8. Cross-sectional views of multi-layer prints under two process conditions and their comparison with an area of 10 mm × 5 mm. (a) and (b) Output from the optimization framework. (c) and (d) Corresponding experimental results. An area of 10 mm × 5 mm in (a) and (b) is the image boundaries, while in (c) and (d) it is marked with white dotted lines.

Table S1

Process parameter windows used for the inconsistency study

Material	Laser power, P, (W)	Scan speed, v, (mm/s)	Powder feed rate, $\dot{m}$, (g/min)	Linear energy density (j × min / mm × g)
316L single-track	300, 450, 600	4, 8, 12	1.4, 2.1, 2.8	8.9-107.1

Table S2

Hyperparameter tuning results for the single-track multi-layer perceptron (MLP) model. Tested are 13 models in three sets of grid search 5-fold cross validation. Tuned hyperparameters include the model architecture (i.e., number of hidden layers and their sizes), the regularization strength, and the learning rate. For each configuration, the mean test score and mean training time are calculated for comparison.

Model	Mean test score (RMSE)	Mean training time (s)	Hidden layers	Regularization strength	Learning rate
1	22.43	12.2	(32)	0.001	0.01
2	21.15	8.7	(32,64)	0.001	0.01
3	21.52	9.0	(32,64,88)	0.001	0.01
4	21.37	48.0	(32,64,128,88)	0.001	0.01
5	20.95	38.0	(32,64,128,256,128,88)	0.001	0.01
6	16.13	167.0	(32,64)	0.1	0.01
7	16.20	243.1	(32,64)	0.001	0.01
8	16.18	254.4	(32,64)	0.0001	0.01
9	16.23	115.4	(32,64)	0.00001	0.01
10	154.97	16.25	(32,64)	0.1	0.0001
11	18.99	16.09	(32,64)	0.1	0.001
12	4.02	16.49	(32,64)	0.1	0.01
13	1.19	16.34	(32,64)	0.1	0.1

Table S3

Hyperparameter tuning results for the multi-track multi-layer perceptron (MLP) model. Tested are 9 models in two sets of grid search 5-fold cross validation. Tuned hyperparameters include the model architecture (i.e., number of hidden layers and their sizes) and the regularization strength. For each configuration, the mean test score and mean training time are calculated for comparison.

Model	Mean test score (R^2)	Mean training time (s)	Hidden layers	Regularization strength
1	0.949	0.740	(8)	10
2	0.949	0.745	(16)	10
3	0.954	0.776	(16,32,16)	10
4	0.953	0.941	(16,32,48,16)	10
5	0.668	0.702	(16,32,48,32,16)	10
6	0.943	0.505	(16,32,16)	100
7	0.953	0.790	(16,32,16)	10
8	0.917	0.888	(16,32,16)	1
9	0.900	0.755	(16,32,16)	0.1

Table S4

Selected model architectures and parameters for the single-track and multi-track machine learning models. The single-track models include the selected models for 316L stainless steel and pure nickel. The parameters shown are the model architecture (i.e., number of hidden layers and their sizes), the regularization strength, the learning rate, and if transfer learning was applied for model training.

Model	Hidden layers	Regularization strength	Learning rate	Model type	Is transfer learning applied?
Single-track model for stainless steel	(32,64)	0.1	0.001	Multi-layer perceptron (MLP)	No
Single-track model for pure nickel	(32,64)	0.1	0.001	Multi-layer perceptron (MLP)	Yes, first layer pre-trained
Multi-track model	(16,32,16)	10	0.001	Multi-layer perceptron (MLP)	No